Pairwise Coding for MIMO-OFDM Visible Light Communication

Pairwise Coding for MIMO-OFDM Visible Light Communication

Hammed G. Olanrewaju, *Student Member, IEEE*, John Thompson, *Fellow, IEEE*, and Wasiu O. Popoola, *Senior Member, IEEE*

***Abstract*—This work proposes a dual pairwise coding (DPWC) technique for multiple-input multiple-output (MIMO) orthogonal frequency division multiplexing (OFDM) based visible light communication (VLC) systems. DPWC is a technique designed to mitigate the signal-to-noise ratio (SNR) imbalance created in the received information symbols due to the light emitting diodes' bandwidth limitations and the strong correlation of typical indoor VLC MIMO channels. With singular value decomposition precoding, the MIMO VLC channel is decomposed into independent parallel sub-channels. The DPWC technique is then applied to further improve the system performance by pairing and interleaving OFDM subcarriers and MIMO sub-channels with imbalanced SNR. The error performance of the proposed DPWC technique is investigated in detail via simulation and experimental demonstration. Its effectiveness with different degrees of bandwidth-limitation (data rate) and channel correlation is presented, and the results are compared with other variants of the pairwise coding technique. DPWC provides performance improvement with a significant reduction in the SNR required to achieve a specific bit error rate (BER).**

***Index Terms*—Visible light communications, optical Multiple-input multiple-output (MIMO), orthogonal frequency division multiplexing (OFDM), precoding, pairwise coding.**

I. Introduction

Visible light communication (VLC) technology using intensity modulated optical sources with direct-detection photodetectors (PDs) has been identified as a promising technology for energy and cost efficient high-speed communication [1]–[3]. Although VLC technology provides access to a huge optical bandwidth resource, the electrical bandwidth of the VLC system is limited to several megahertz by the front-end devices, i.e., light emitting diodes (LEDs) [4], [5]. As a result, spectrally efficient modulation techniques such as pulse-amplitude modulation (PAM) [6] and optical Orthogonal frequency division multiplexing (OFDM) [7] have been explored to increase throughput. Moreover, Multiple-input multiple-output (MIMO) schemes using multiple LEDs and PDs to exploit additional degree of freedom, such as space and emitted colour of the optical sources and field of view of detectors are also prime candidates for improving the capacity and/or reliability of VLC systems [8], [9].

In a spatial-multiplexing MIMO-OFDM VLC system, the performance of the system is highly dependent on the degree of the undesirable correlation among the spatially separated signals. The MIMO channel matrix can be highly correlated in an indoor VLC systems with direct line-of-sight (LoS) [5]. This limits the achievable multiplexing gain. Therefore, MIMO systems utilizing singular value decomposition (SVD) have been proposed to enhance system performance when channel state information (CSI) is known at the transmitter and receiver [10], [11]. The SVD architecture transforms the MIMO channel matrix into a set of parallel independent sub-channels (SCHs) and it provides significant diversity gain [12], [13].

In an SVD-based MIMO-OFDM VLC system, the stronger the channel correlation, the more spread out the gains (singular values) of the independent SCHs created by the SVD, and the poorer the system performance [12]. The degree of channel correlation is quantified by the condition number, η, of the channel matrix, i.e., the ratio of the maximum to the minimum gains (singular values) of the independent SCHs. The stronger the channel correlation, the higher the value of η, and the bigger the imbalance between the gains of the SCHs. Similarly, the bandwidth limitation of the LEDs leads to frequency selective fading such that the subcarriers (SCs) in an OFDM frame are attenuated differently. This creates an imbalance in the received signal to noise ratios (SNR) of the SCs, and since the overall system performance is averaged across the SCs, then the system performance is limited by the SCs with degraded SNR.

In this paper, we implement joint coding of paired information symbols to mitigate the effect of the LEDs' bandwidth limitation and the strong correlation of the indoor VLC channel [8]. This coding technique, termed pairwise coding (PWC), also known as Signal space diversity (SSD) [14], is based on the rotated symbol constellation, and it is an effective method of improving overall system performance when an SNR imbalance exists between channels [13], [15]–[20]. In radio frequency communication over Rayleigh fading channels, PWC technique is applied to improve the diversity gain of single-input-single-output (SISO) systems in [14] and single-carrier MIMO systems in [13], [19], [20]. Spatial multiplexing based MIMO system is considered in [13], while the authors of [19] explored PWC to achieve transmit diversity and enhance the error performance of spatial modulation based MIMO systems. The concept of PWC is also explored in [20] to improve the error performance of MIMO transmission in combination with zero-forcing beamforming, while [21] considered co-ordinate interleaving of symbols over eigenchannels of MIMO systems for diversity-multiplexing trade-off. In [22], the idea of rotational modulation and component interleaver

H. G. Olanrewaju, J. Thompson and W. O. Popoola are with the School of Engineering, Institute for Digital Communications, LiFi R&D Centre, The University of Edinburgh, UK. E-mail: {g.olanrewaju, john.thompson and w.popoola}@ed.ac.uk. This work is supported by the Petroleum Technology Development Fund (PTDF) of the Federal government of Nigeria.

similar to PWC is employed to obtain modulation diversity gain in MIMO-OFDM scheme for wireless local area networks (WLAN) technology. PWC has also been applied in optical OFDM over fibre channels to improve receiver sensitivity and reduce carrier power [15], to mitigate Polarization dependent loss (PDL) [23] and to decrease dispersion-induced power fading [17]. In SISO VLC systems, an adaptive scheme which combines PWC with selective SC loading is proposed in [24]. The merit of PWC is that for large SNR imbalance, significant improvement in system performance in terms of error rate, throughput or reliability can be achieved without additional power or bandwidth requirement.

This paper provides the following novel contributions: we propose and demonstrate a dual PWC (DPWC) scheme in which PWC is applied across two degrees of freedom, i.e., spatial and spectral dimensions, of a MIMO-OFDM VLC system, and its error performance is investigated. An indoor MIMO-OFDM VLC system is modelled taking into account the LED frequency selective response, and correlation of the line-of-sight (LoS) channel response of multiple LEDs/PDs links. SVD-based precoding is employed to optimize the system and PWC coding is then applied to further enhance system error performance by mitigating the effect of SNR imbalance across OFDM SCs and MIMO SCHs. The bit error rate (BER) plots show that high performance gains are achieved by applying DPWC compared to using only SVD precoding. Also, the DPWC scheme is compared with other variants of the PWC techniques in which SNR imbalance is considered in only the spatial or spectral domain. The performance gains in terms of SNR are shown for different degrees of bandwidth limitation and MIMO channel conditions. Furthermore, the performance of the proposed DPWC scheme is validated with experimental demonstration. Error performance results are shown for MIMO channels with different condition number and at varying data rates.

The remainder of this paper is organized as follows. The system model and the SVD precoding scheme for the MIMO-OFDM VLC system are presented in Section II. The encoding and decoding process for the PWC technique are then proposed in Section III. In Section IV, the results of the performance evaluation via simulations are presented and discussed. The experimental setup and results are provided in Section V, while Section VI gives the concluding remarks.

Notations: the superscripts ^{T} and * denote the transposition and Hermitian transposition, respectively. An $n \times n$ identity matrix is denoted by $\mathbf{I}_n$. Also, the operators $\Re(\cdot)$ and $\Im(\cdot)$ provide the real and imaginary parts of a complex argument, while $\widehat{i} = \sqrt{-1}$ is the imaginary unit.

II. SYSTEM MODEL AND SVD PRECODING FOR MIMO-OFDM VLC

We consider a MIMO-OFDM VLC system using N_{T} LEDs and N_{R} PDs for spatial multiplexing, where $N_{\mathrm{T}} \leq N_{\mathrm{R}}$. The system block diagram is shown in Fig. 1. By using the OFDM technique, the frequency band of each MIMO transmitter SCH is divided into N_{K} SCs, out of which N_{D} are data-carrying SCs on which information symbols are conveyed, while the rest are used as null SCs or Hermitian conjugate SCs which are required to obtain real-valued time domain signals for VLC system. At the transmitter, first, the information bits are mapped into a specific M-level quadrature amplitude modulation (QAM) symbol constellation. Then, a serial-to-parallel (S/P) block converts the entire symbol stream into blocks of $N_{\mathrm{T}} \times N_{\mathrm{D}}$ complex symbols which are assigned to the N_{D} data-carrying SCs in the OFDM frames sent by the N_{T} LEDs. The symbol-to-subcarrier mapping is then followed by the DPWC and SVD precoding of the information symbols. These two transmitter operations along with the symbol detection at the receiver requires CSI at the transmitter and receiver. Consequently, before data transmission, the CSI is first obtained via an initial channel training using pilot/training symbols. The block-type pilot arrangement is used such that the training OFDM frames sent by the N_{T} LEDs have pilot symbols at all SCs. At receiver, the frequency-domain MIMO channel coefficients at each SC are obtained based on a priori knowledge of the pilot symbols by using least squares (LS) estimation technique [25]. The estimated $N_{\mathrm{R}} \times N_{\mathrm{T}}$ frequency-domain MIMO channel coefficients for the k-th SC is denoted by $\mathbf{H}_k = [h^k_{i,j}]$, for $i = 1 \ldots N_{\mathrm{R}}$, $j = 1 \ldots N_{\mathrm{T}}$, $k = 1, \ldots, N_{\mathrm{D}}$, where $h^k_{i,j}$ corresponds to the channel coefficient of k-th OFDM SC between the j-th LED and the i-th PD. We note that the entries of the channel matrix $\mathbf{H}_k = [h^k_{i,j}]$ corresponds to the products of the gain of the optical wireless channel and the gain of the SC from the frequency response of each LED.

The CSI obtained from the training symbols are then used at the transmitter to implement DPWC and SVD precoding in that order. In the implementation of DPWC technique which will be discussed subsequently in Section III, the SCs/SCHs are paired based on their gains (SNR values). By applying SVD precoding, these SC/SCH gains are equivalent to the singular values obtained from the SVD of the channel matrix. Hence, the SVD computation of the channel matrix is first obtained in order to determine how the SCs/SCHs are paired when applying DPWC. The SVD computation is expressed as [12]:

$$\mathbf{H}_k = \mathbf{U}_k \mathbf{\Lambda}_k \mathbf{V}^*_k \tag{1}$$

where $\mathbf{U}_k$ and $\mathbf{V}_k$ are unitary matrices of dimensions $N_{\mathrm{R}} \times N_{\mathrm{R}}$ and $N_{\mathrm{T}} \times N_{\mathrm{T}}$ respectively. The matrix $\mathbf{\Lambda}_k$ is the $N_{\mathrm{R}} \times N_{\mathrm{T}}$ rectangular diagonal matrix of the ordered non-negative singular values, i.e., $\lambda_{1,k} \geq \lambda_{2,k} \cdots \geq \lambda_{N_{\mathrm{T}},k} > 0$. Considering the k-th SC, let the N_{T}-dimensional vector of DPWC encoded symbols be defined as $\mathbf{x}_k$, the output of SVD precoding is then given by:

$$\overline{\mathbf{x}}_k = \mathbf{V}_k \, \mathbf{x}_k \tag{2}$$

where $\mathbf{V}_k$ is applied as the SVD precoding matrix. For VLC using intensity modulation and direct detection (IM/DD), real-valued time domain signals are required to modulate the LEDs' intensity. Hence, Hermitian symmetry is preserved during the symbol-to-subcarrier mapping such that the symbols on the negative-frequency SCs are set to the complex conjugate of the precoded symbols assigned to the positive-frequency SCs. In this way, the inverse fast Fourier transform (IFFT) operation yields real-valued time domain signal. After adding

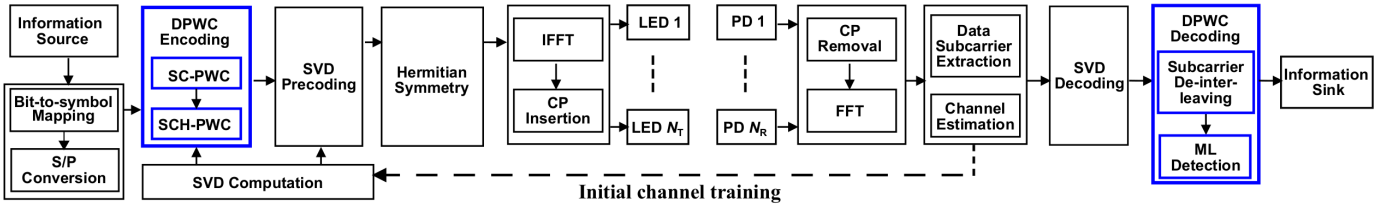

Fig. 1: Block diagram of MIMO-OFDM based VLC system

cyclic prefix (CP), a suitable direct-current (DC) level is also added to obtain positive-valued signal which is then used to modulate the intensity of the LEDs.

At the receiver, the opto-electrical conversion of the incoming optical radiation is achieved using PDs. After post detection amplification and analogue-to-digital (A/D) conversion, the CP is removed and an FFT operation translates the received signal into its frequency domain equivalent. Then, the precoded data symbols are extracted from the data-carrying SCs. As stated above, for IM/DD VLC systems, the time-domain transmitted and received signals as well as the channel and LED impulse responses are real-valued [7], [26]. Thus, in the frequency domain representation of the signals and the channel coefficients, the conjugate SCs on the negative frequencies are mirror images of the data-carrying SCs. Therefore, in the following analysis, we will focus on the data-carrying SC. The N_{R}-dimensional vector of received symbols on the k-th data-carrying SC (in the frequency domain) is given by:

$$\mathbf{y}_k \;=\; \mathbf{H}_k\,\overline{\mathbf{x}}_k + \mathbf{n}_k \;=\; \mathbf{H}_k\mathbf{V}_k\,\mathbf{x}_k + \mathbf{n}_k \tag{3}$$

where $\mathbf{n}_k$ is the independent and identically distributed additive Gaussian noise vector with variance, σ_n^2. The received symbols on each SC is then decomposed into independent parallel SCHs by multiplying with the SVD decoding matrix, $\mathbf{U}_k^*$, and we obtain:

$$\begin{aligned}\mathbf{r}_k \;&= \mathbf{U}_k^*\,\mathbf{y}_k = \;\mathbf{U}_k^*\mathbf{H}_k\mathbf{V}_k\mathbf{x}_k + \mathbf{U}_k^*\mathbf{n}_k \\ &= \;\mathbf{\Lambda}_k\mathbf{x}_k + \mathbf{z}_k.\end{aligned} \tag{4}$$

where $\mathbf{r}_k = [r_{1,k}, \ldots, r_{N_{\mathrm{T}},k}]^T$ is the received symbol vector at the output of the SVD decoder. The final expression in (4) is obtained by exploiting the unitary properties of $\mathbf{U}_k$ and $\mathbf{V}_k$, i.e., $\mathbf{U}_k^*\mathbf{U}_k = \mathbf{I}_{N_{\mathrm{R}}}$ and $\mathbf{V}_k^*\mathbf{V}_k = \mathbf{I}_{N_{\mathrm{T}}}$. The Gaussian noise vector $\mathbf{z}_k = \mathbf{U}_k^*\mathbf{n}_k$ has the same statistics as $\mathbf{n}_k$, i.e., the noise variance $\sigma_z^2 = \sigma_n^2$. The estimates of the transmitted symbols are then obtained via the joint PWC decoding and MLD process detailed in the subsequent section. Given that $\mathbf{\Lambda}_k$ is a diagonal matrix, then the expression in (4) represents the decomposition of the MIMO channels of each SC into N_{T} independent parallel SCHs. Therefore, for the SVD-based MIMO-OFDM system, the received symbol from the j-th transmitter SCH (LED) and the k-th OFDM SC is given by:

$$r_{j,k} = \lambda_{j,k}x_{j,k} + z_{j,k}. \tag{5}$$

Consequently, the singular value, $\lambda_{j,k}$ corresponds to the equivalent channel gain associated with the information symbol transmitted on the k-th SC by the j-th LED (transmitter SCH). From (5), the received SNR of the SCs on each of the independent SCHs created by the SVD precoding is a factor of the combined SC and SCH gain, and it is given by $\gamma_{j,k} = \lambda_{j,k}^2|s_{j,k}|^2/\sigma_z^2$. This aligns with our previous statement that the SC/SCH gains are equivalent to the singular values obtained from the SVD of the channel matrix.

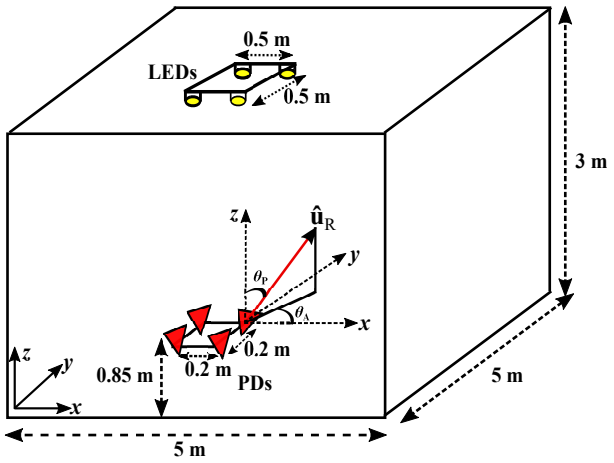

Fig. 2: Geometry of the indoor MIMO VLC system

VLC Channel Model

The overall system response includes the LoS channel impulse response of multiple LEDs and PDs, and the band-limited LED response. The LEDs' frequency response is modelled by a first order Butterworth low-pass filter (LPF) [27], [28]. The 3 dB bandwidth of the LEDs is set to be $B_{\mathrm{LED}} = 15$ MHz (which is the measured 3 dB bandwidth of the experimental VLC link, see Fig. 10). The configuration of the indoor MIMO VLC link in a typical $5 \times 5 \times 3$ m room is depicted in Fig. 2. In a 4×4 MIMO-OFDM system, the four LEDs are mounted on ceiling facing downward at 3 m above the floor, while the receiver plane is 0.85 m away from the floor. The VLC channel is simulated based on the source and receiver models in [29] and the simulation parameters used are provided in Table I. Angular diversity is employed at the receiver to optimize the incident angle of the emitted intensity by varying polar and azimuthal angles of the PDs. Thus, using Fig. 2, the orientation vector of the PDs are given by $\hat{\mathbf{u}}_{\mathrm{R}} = [\sin\theta_{\mathrm{A}}\sin\theta_{\mathrm{P}},\ \sin\theta_{\mathrm{A}}\sin\theta_{\mathrm{P}},\ \cos\theta_{\mathrm{A}}\cos\theta_{\mathrm{P}}]$ where θ_{A} is the azimuth angle on x-y plane and θ_{P} is the polar angle from the z-axis. The orientation vector of the LEDs which are facing downward vertically is obtained as $\hat{\mathbf{u}}_{\mathrm{T}} = [0, 0, -1]$. Using the azimuth angles of 45°, 135°, 225° and 315° for the four PDs, we obtain the optimal polar angles which ensure LoS

TABLE I: VLC CHANNEL SIMULATION PARAMETERS

Parameter	Value
LED beaming angle Φ	15° to 35°
LED separation	0.5 m
PD field of view	60°
PD separation	0.2 m
PD Area (cm^2)	1.0
Gain of optical filter	1.0
Concentrator refractive index	1.5
LEDs' coordinates (m)	(1.75,1.75,3), (1.75,2.25,3) (2.25,1.75,3), (2.25,2.25,3)
PDs' coordinates (m)	(1.9,1.9,0.85), (1.9,2.1,0.85) (2.1,1.9,0.85), (2.1,2.1,0.85)

channel gain to all the PDs and minimizes the off-diagonal values (cross channel gains) of the MIMO channel matrix.

III. PAIRWISE CODING FOR MIMO-OFDM VLC

The PWC technique entails a joint coding of paired information symbols over the spectral and/or the spatial dimensions. This process of encoding symbols with PWC is illustrated in Fig. 3 using 4-QAM. First, the information bits to be modulated onto a pair of SCs/SCHs are mapped into two complex QAM constellations, $\alpha = \alpha_{\rm r} + \widetilde{i}\alpha_{\rm i}$ and $\beta = \beta_{\rm r} + \widetilde{i}\beta_{\rm i}$, where $\alpha_{\rm r}$ and $\beta_{\rm r}$ denote the real, i.e., in-phase (I) components, while $\alpha_{\rm i}$ and $\beta_{\rm i}$ denote the imaginary, i.e., quadrature (Q) components. Then, a phase shift, ψ is applied to both constellations to obtain $\alpha_{\rm rot}$ and $\beta_{\rm rot}$ respectively. The phase rotation is then followed by I/Q component interleaving to generate the complex constellations $\alpha_{\rm int}$ and $\beta_{\rm int}$ transmitted on each SC/SCH.

This interleaving process transfers the SNR imbalance between the paired SC/SCH to the I and Q components of the symbols modulated onto the SCs/SCHs, while the phase rotation transforms the classical symbol constellations such that the minimum distance between the received symbols is increased [13], [14]. Thus, with additive Gaussian noise, the ML detection error is reduced by increasing the minimum distance. The concept of phase rotation is illustrated in Fig. 4 with the diagram of classical (un-rotated) and rotated constellations for 4-QAM. With I/Q component interleaving, only one of the I/Q components is received with low SNR. As shown in Fig. 4a, for classical constellations, when the original constellation points (filled circles) are compressed due to low SNR on, say, the Q component, then the minimum distance between any two received compressed points (empty circles) is reduced. It is possible for any two received points to merge together with zero minimum distance and thereby causing poor error performance. In contrast, for the rotated constellations in Fig. 4b, it can be seen that a non-zero minimum distance holds for the received points since no two points merges. Thus, making the rotated constellation more robust against the effects of noise.

When PWC is applied across the OFDM SCs (spectral dimension), the PWC scheme is termed Subcarrier PWC (SC-PWC), and when PWC is applied over the transmitter SCHs (spatial dimension), it is referred to as Subchannel PWC (SCH-PWC). The generalised case is the dual PWC (DPWC)

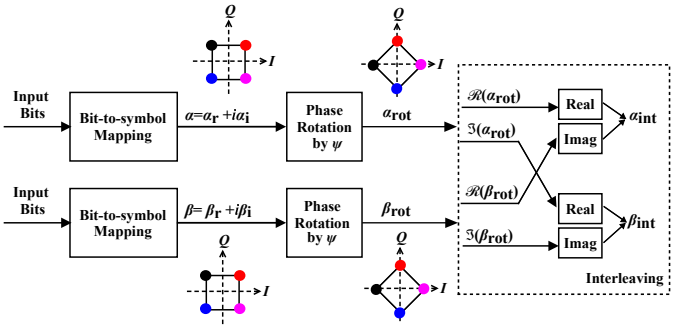

Fig. 3: Illustration of pairwise coding technique. The operators $\Re(\cdot)$ and $\Im(\cdot)$ provide the real and imaginary parts of a complex argument.

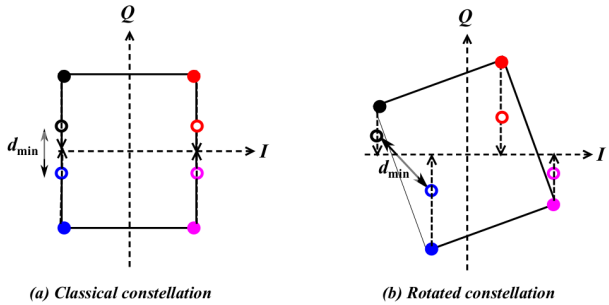

Fig. 4: Illustration of the effect of phase rotation in PWC: (a) classical (un-rotated) constellation diagram (b) rotated constellation diagram ($\psi = 20^\circ$). The empty circles denote compressed constellation points due to low SNR of the Q-component, while the filled circles denote original (uncompressed) constellation. $d_{\rm min}$ denote the minimum distance between constellation points.

and it involve applying PWC across the OFDM SCs and over the transmitter SCHs. Thus, the SC-PWC and SCH-PWC schemes are regarded as subsets of DPWC. In this paper, the emphasis is on the DPWC scheme which is employed to make the MIMO-OFDM VLC system robust against the frequency-selective response of the LEDs (in spectral dimension) and the correlation of the optical wireless channel (in spatial dimension). The SC-PWC and SCH-PWC schemes are treated as special cases of DPWC.

The DPWC encoding starts with the pairing of one OFDM SC having low SNR with another having high SNR. This is followed by the phase rotation and interleaving of the in-phase (I) and quadrature (Q) components of the information symbols on the paired SCs. A similar procedure is then followed to encode the information symbols on the transmitter SCHs. The DPWC encoding can also be implemented in reverse order by starting with the phase rotation and interleaving across the SCHs, before performing similar operations on the OFDM SCs. In the following, we describe the encoding process for implementing SC-PWC and SCH-PWC, and how both schemes are integrated into a single DPWC technique for MIMO-OFDM VLC systems. Later, we outline the procedure for decoding and estimating the transmitted symbols from the received signal.

A. DPWC Encoding

To implement DPWC encoding, the information symbols to be modulated onto the data-carrying SCs are first encoded with SC-PWC, then the SCH-PWC is applied to the SC-PWC encoded symbols.

1) SC-PWC Encoding: Without loss of generality, we assume that N_{D} is an even number, and that the LEDs have similar frequency response profile, with the data-carrying SCs arranged in descending order of their channel gains, i.e., $\lambda_{j,1} \geq \lambda_{j,2} \cdots \geq \lambda_{j,N_{\mathrm{D}}}$, for $j \in [1, N_{\mathrm{T}}]$. The M-QAM information symbols mapped to the k-th SC for the N_{T} LEDs is defined by $\mathbf{s}_k = [s_{1,k}, \ldots, s_{N_{\mathrm{T}},k}]^T$ Based on their gain, the N_{D} data-carrying SCs are grouped into two sets: those with high gains/SNR (good SCs), denoted by $\{\ell_p\}$, and those with small gains/SNR (bad SCs), denoted by $\{m_p\}$, where the pairing index, $p = 1, \ldots, N_{\mathrm{D}}/2$. The indices of the SCs corresponding to the p-th pair of good and bad SCs is given by: $(\ell_p, m_p) = (p, N_{\mathrm{D}} - p + 1)$. Hence, the vectors of information symbols mapped onto this pair of SCs are given by $(\mathbf{s}_{\ell_p}, \mathbf{s}_{m_p})$. After pairing, a constant phase shift, $\mathbf{\Psi}_p, \forall\, p$, is applied to the symbol vectors on the p-th SC pair, and the rotated symbol vectors are obtained as:

$$(\mathbf{s}^{\mathrm{rot}}_{\ell_p},\, \mathbf{s}^{\mathrm{rot}}_{m_p}) \;= (e^{\widehat{i\mathbf{\Psi}_p}}\, \mathbf{s}_{\ell_p},\, e^{\widehat{i\mathbf{\Psi}_p}}\, \mathbf{s}_{m_p}), \tag{6}$$

where $\mathbf{\Psi}_p = \mathrm{diag}(\Psi_{1,p}, \ldots, \Psi_{N_{\mathrm{T}},p})$ is a diagonal matrix whose non-zero diagonal elements $\Psi_{j,p}\, \forall j$, denote the phase shift applied to the p-th SC pair on the j-th SCH. Next, I/Q component interleaving is applied over the rotated symbol vectors, and this entails exchanging the imaginary part of $\mathbf{s}^{\mathrm{rot}}_{\ell_p}$ and the real part of $\mathbf{s}^{\mathrm{rot}}_{m_p}$ [14]. The I/Q interleaving yields the two SC-PWC encoded symbol vectors on the p-th SC pair as:

$$\mathbf{w}_{\ell_p} \;=\; \Re(\mathbf{s}^{\mathrm{rot}}_{\ell_p}) + \Re(\mathbf{s}^{\mathrm{rot}}_{m_p}) = \; \Re(e^{\widehat{i\mathbf{\Psi}_p}}\, \mathbf{s}_{\ell_p}) + \Re(e^{\widehat{i\mathbf{\Psi}_p}}\, \mathbf{s}_{m_p}) \tag{7}$$

$$\mathbf{w}_{m_p} = \Im(\mathbf{s}^{\mathrm{rot}}_{\ell_p}) + \Im(\mathbf{s}^{\mathrm{rot}}_{m_p}) = \Im(e^{\widehat{i\mathbf{\Psi}_p}}\, \mathbf{s}_{\ell_p}) + \Im(e^{\widehat{i\mathbf{\Psi}_p}}\, \mathbf{s}_{m_p}) \tag{8}$$

The phase rotation (in (6)) and I/Q interleaving (in (7) and (8)) involved in the SC-PWC encoding can be combined into matrix-multiplication with an orthogonal matrix as:

$$\begin{bmatrix} \Re(\mathbf{w}_{\ell_p}) & \Im(\mathbf{w}_{\ell_p}) \\ \Re(\mathbf{w}_{m_p}) & \Im(\mathbf{w}_{m_p}) \end{bmatrix} = \begin{bmatrix} \cos \mathbf{\Psi}_p & -\sin \mathbf{\Psi}_p \\ \sin \mathbf{\Psi}_p & \cos \mathbf{\Psi}_p \end{bmatrix} \times \begin{bmatrix} \Re(\mathbf{s}_{\ell_p}) & \Re(\mathbf{s}_{m_p}) \\ \Im(\mathbf{s}_{\ell_p}) & \Im(\mathbf{s}_{m_p}) \end{bmatrix} \tag{9}$$

The proof of (9) is provided in Section A of the Appendix.

2) SCH-PWC Encoding: The SCH-PWC encoding is performed over the transmitter SCHs in a similar manner to the SC-PWC encoding of the OFDM SCs. With the SVD of the channel matrix, the channel gain obtained for the transmitter SCHs on the k-th SC are arranged in descending order. Therefore, considering an even N_{T}, by pairing the SCHs which have high gain/SNR with those with small gain/SNR, the SCHs pairing list is given by $(c_q, d_q) = (q, N_{\mathrm{T}} - q + 1)$ for $q = 1, \ldots, N_{\mathrm{T}}/2$, where c_q denote the index of high-gain SCHs while d_q denote the index of the small-gain SCHs. The corresponding SC-PWC encoded complex symbols mapped onto the paired SCHs are represented by $w_{c_q,k}$ and $w_{d_q,k}$. After pairing, phase rotation and I/Q component interleaving are applied to symbols $w_{c_q,k}$ and $w_{d_q,k}$. The phase rotation and component interleaving involved in SCH-PWC encoding of the q-th pair of SCHs can be parameterised by the orthogonal matrix (SCH-PWC encoding matrix) [13]:

$$\mathbf{\Omega}_{q,k} = \begin{bmatrix} \Omega^{q,k}_{1,1} & \Omega^{q,k}_{1,2} \\ \Omega^{q,k}_{2,1} & \Omega^{q,k}_{2,2} \end{bmatrix} = \begin{bmatrix} \cos \phi_{q,k} & -\sin \phi_{q,k} \\ \sin \phi_{q,k} & \cos \phi_{q,k} \end{bmatrix}, \tag{10}$$

where $\phi_{q,k}$ is the angle by which the symbol on the q-th SCH pair of the k-th OFDM SC are rotated. Therefore, by applying SCH-PWC encoding, the DPWC encoded symbols on the q-th SCH pair are given by:

$$\begin{bmatrix} x_{c_q,k} \\ x_{d_p,k} \end{bmatrix} = \mathbf{\Omega}_{q,k} \times \begin{bmatrix} w_{c_q,k} \\ w_{d_p,k} \end{bmatrix}. \tag{11}$$

The SCH-PWC encoding process expressed by (11) translates to performing I/Q component interleaving and phase rotation of the complex symbol. The proof of this is provided in Section B of the Appendix. Using (11), the SCH-PWC encoding of all the N_{T} SCHs on the k-th SC can be written as:

$$\mathbf{x}_k \;= \mathbf{\Xi}_k\, \mathbf{w}_k, \tag{12}$$

where $\mathbf{\Xi}_k = \{\xi^k_{i,j}\}$ denote the $N_{\mathrm{T}} \times N_{\mathrm{T}}$ generalised SCH-PWC encoding matrix for all the N_{T} transmit SCHs on the k-th SC. Thus, the matrix $\mathbf{\Omega}_{q,k}$ corresponds to a sub-matrix of $\mathbf{\Xi}_k$, and the latter can be obtained from the former as follows:

$$\begin{aligned} \xi^k_{c_q,c_q} &= \Omega^{q,k}_{1,1}; \quad \xi^k_{c_q,d_q} = \Omega^{q,k}_{1,2} \\ \xi^k_{d_q,c_q} &= \Omega^{q,k}_{2,1}; \quad \xi^k_{d_q,d_q} = \Omega^{q,k}_{2,2}. \end{aligned} \tag{13}$$

We note that the $N_{\mathrm{T}} \times N_{\mathrm{D}}$ matrices of the user's information symbols and the DPWC encoded symbols are denoted by $\mathbf{S} = [\mathbf{s}_1, ..., \mathbf{s}_k, ..., \mathbf{s}_{N_{\mathrm{D}}}]$ and $\mathbf{X} = [\mathbf{x}_1, ..., \mathbf{x}_k, ..., \mathbf{x}_{N_{\mathrm{D}}}]$ respectively. The vectors $\mathbf{s}_k$ and $\mathbf{x}_k$ are the k-th columns (i.e., the k-th SC) of $\mathbf{S}$ and $\mathbf{X}$ respectively.

From (9) and (11), it can seen that the encoding process for the DPWC scheme can be defined completely in terms of the rotation angles. Hence, the design of the PWC technique is essentially dependent on using the optimal angles that maximize the minimum distance between the paired symbols constellations, which in turn minimizes the average error probability. For an M-QAM symbol constellation, by maximizing the mutual information between a pair of information symbol vectors [13], the optimal rotation angles for SC-PWC encoding and SCH-PWC are given by (14) and (15), respectively.

The optimal angles in (14) and (15) are obtained by testing each candidate pair of (μ, υ) in set $\mathbb{S}_M$. However, since CSI is known at the transmitter, these computations can be performed before transmitting the user data.

As stated above, the SC-PWC and SCH-PWC schemes can be treated as subsets of the DPWC scheme. Thus, by setting $\mathbf{\Xi} = \mathbf{I}_{N_{\mathrm{T}}}$, the DPWC scheme becomes an SC-PWC scheme with PWC applied across the OFDM SCs only. Also, by setting $\mathbf{w}_k = \mathbf{s}_k,\ \forall\, k$, we derive the SCH-PWC scheme in which PWC is applied across the transmitter SCHs only. Furthermore, (9) and (11) indicate that DPWC encoding can be expressed in terms of multiplication with orthogonal matrices

$$\Psi_{j,p}^{\text{opt}} \;=\; \arg \max_{\Psi_{j,p}\in[0,\pi/4]} \left[\min_{(\mu,\upsilon)\in\mathbb{S}_M} \left[(\mu^2+\upsilon^2) \left(\lambda_{j,\ell_p}^2 \cos^2\left(\Psi_{j,p}-\varphi_{\mu,\upsilon}\right) + \lambda_{j,m_p}^2 \sin^2\left(\Psi_{j,p}-\varphi_{\mu,\upsilon}\right) \right) \right] \right] \tag{14}$$

$$\phi_{q,k}^{\text{opt}} \;=\; \arg \max_{\phi_{q,k}\in[0,\pi/4]} \left[\min_{(\mu,\upsilon)\in\mathbb{S}_M} \left[(\mu^2+\upsilon^2) \left(\lambda_{c_q,k}^2 \cos^2\left(\phi_{q,k}-\varphi_{\mu,\upsilon}\right) + \lambda_{d_q,k}^2 \sin^2\left(\phi_{q,k}-\varphi_{\mu,\upsilon}\right) \right) \right] \right], \tag{15}$$

where

$$\mathbb{S}_M \triangleq \{(\mu,\upsilon) \,|\, |\mu|, |\upsilon| \in [0, \sqrt{M}-1],\ (\mu,\upsilon) \neq (0,0)\}, \tag{16}$$

$$\varphi_{\mu,\upsilon} = \tan^{-1}\left(\frac{\upsilon}{\mu}\right). \tag{17}$$

which can be readily inverted by finding its transpose.

B. PWC Decoding and Maximum Likelihood Detection

At the receiver, with DPWC encoding applied at the transmitter, the expression in (4), for the received symbol vector on the k-th SC, becomes:

$$\begin{aligned} \mathbf{r}_k &= \mathbf{\Lambda}_k\, \mathbf{x}_k + \mathbf{z}_k \;= \mathbf{\Lambda}_k\, \mathbf{\Xi}_k\, \mathbf{w}_k + \mathbf{z}_k \\ &= \mathbf{G}_k\, \mathbf{w}_k + \mathbf{z}_k \end{aligned} \tag{18}$$

where $\mathbf{G}_k = \mathbf{\Lambda}_k\, \mathbf{\Xi}_k$ is the effective channel gain matrix for the k-th SC. Next, the PWC decoding process is done on a per SC basis by first de-interleaving the I and Q components of received symbols on the paired SCs. That is, for the p-th SC pair, (ℓ_p, m_p), the de-interleaved complex symbols are obtained as:

$$\begin{aligned} \widetilde{\mathbf{r}}_{\ell_p} &= \mathbf{G}_{\ell_p} \Re(\mathbf{s}_{\ell_p}^{\text{rot}}) + \Re(\mathbf{z}_{\ell_p}) + \widehat{i}(\mathbf{G}_{m_p} \Im(\mathbf{s}_{\ell_p}^{\text{rot}}) + \Re(\mathbf{z}_{m_p})) \\ &= \mathbf{G}_{\ell_p} \Re(e^{\widehat{i}\mathbf{\Psi}_p}\mathbf{s}_{\ell_p}) + \Re(\mathbf{z}_{\ell_p}) \;+\; \widehat{i}(\mathbf{G}_{m_p} \Im(e^{\widehat{i}\mathbf{\Psi}_p}\mathbf{s}_{\ell_p}) \\ &\qquad + \Re(\mathbf{z}_{m_p})) \end{aligned} \tag{19}$$

$$\begin{aligned} \widetilde{\mathbf{r}}_{m_p} = \mathbf{G}_{\ell_p} \Re(e^{\mathbf{\Psi}_p}\mathbf{s}_{m_p}) + \Im(\mathbf{z}_{\ell_p}) \;+\; \widehat{i}(\mathbf{G}_{m_p} \Im(e^{\widehat{i}\mathbf{\Psi}_p}\mathbf{s}_{m_p}) \\ + \Re(\mathbf{z}_{m_p})) \end{aligned} \tag{20}$$

The interpretation of (19) is that due to the I/Q interleaving of the paired SC at the transmitter, the I and Q components of the rotated symbol constellation on SC ℓ_p are transmitted though separate SCs with different gains/SNRs. That is, the real component, $\Re(e^{\mathbf{\Psi}_p}\mathbf{s}_{\ell_p})$ is sent on SC ℓ_p with effective channel gain matrix, $\mathbf{G}_{\ell_p}$, while the imaginary component, $\Im(e^{\mathbf{\Psi}_p}\mathbf{s}_{\ell_p})$, is sent via SC m_p which has an effective channel gain matrix $\mathbf{G}_{m_p}$. The noise vectors $\Re(\mathbf{z}_{\ell_p})$ and $\Re(\mathbf{z}_{m_p})$ are the respective noise terms associated with the real and imaginary components of the de-interleaved symbol $\widetilde{\mathbf{r}}_{\ell_p}$. A similar interpretation also holds for (20).

The MLD estimates of the transmitted symbols on the p-th SC pair are given by:

$$\begin{aligned} \widehat{\mathbf{s}}_{\ell_p} &= \arg \min_{\mathbf{a}\,\in\,\mathcal{A}^{N_\text{T}}} \left\{ \|\widetilde{\mathbf{r}}_{\ell_p} - \mathbf{a}_{\ell_p}^{\text{rot}}\|^2 \right\} \\ \widehat{\mathbf{s}}_{m_p} &= \arg \min_{\mathbf{a}\,\in\,\mathcal{A}^{N_\text{T}}} \left\{ \|\widetilde{\mathbf{r}}_{m_p} - \mathbf{a}_{m_p}^{\text{rot}}\|^2 \right\} \end{aligned} \tag{21}$$

where $\|\cdot\|$ denote the Euclidean norm operator, $\mathbf{a}$ is an $N_\text{T}\times 1$ vector of M-QAM constellations drawn from the set $\mathcal{A}^{N_\text{T}}$, and $\mathbf{a}_{\ell_p}^{\text{rot}}$ and $\mathbf{a}_{m_p}^{\text{rot}}$ are the rotated and scaled constellations obtained from:

$$\begin{aligned} \mathbf{a}_{\ell_p}^{\text{rot}} &= \mathbf{G}_{\ell_p} \Re(e^{\widehat{i}\mathbf{\Psi}_p}\mathbf{a}) + \widehat{i}\mathbf{G}_{m_p} \Im(e^{\widehat{i}\mathbf{\Psi}_p}\mathbf{a}) \\ \mathbf{a}_{m_p}^{\text{rot}} &= \mathbf{G}_{\ell_p} \Re(e^{\widehat{i}\mathbf{\Psi}_p}\mathbf{a}) + \widehat{i}\mathbf{G}_{m_p} \Im(e^{\widehat{i}\mathbf{\Psi}_p}\mathbf{a}). \end{aligned} \tag{22}$$

The set $\mathcal{A}^{N_\text{T}}$ is the Cartesian product of N_T sets of M-QAM constellations $\mathcal{A}$. The MLD expressed by (21) simultaneously estimates the N_T transmitted symbols modulated unto SCs ℓ_p and m_p of the OFDM frames sent on all the N_T transmitter SCHs. Thus, the ML search is performed over a $2N_\text{T}$ dimensional signal space. This can be reduced significantly into $N_\text{T}/2$ independent MLD steps over a 4-D signal space by performing MLD over one pair of SCHs at a time. For instance, considering the q-th SCH pair, i.e., (c_q, d_q), let $\mathbf{G}_{\ell_p,q}$ and $\mathbf{\Psi}_{p,q}$ denote the 2×2 sub-matrices consisting of the entries in the c_q and d_q rows and columns of the matrices $\mathbf{G}_{\ell_p}$ and $\mathbf{\Psi}_p$ respectively. Also, let $\widehat{\mathbf{s}}_{\ell_p,q}$ and $\widetilde{\mathbf{r}}_{\ell_p,q}$ denote the 2×1 vectors consisting of the entries in rows c_q and d_q of the vector $\widehat{\mathbf{s}}_{\ell_p,q}$ and $\widetilde{\mathbf{r}}_{\ell_p}$ respectively. Then, the MLD estimates of the symbols modulated onto SCs ℓ_p and m_p, and sent over transmitter SCHs c_q and d_q are obtained from (21) as:

$$\begin{aligned} \widehat{\mathbf{s}}_{\ell_p,q} &= \arg \min_{\widetilde{\mathbf{a}}\,\in\,\mathcal{A}^2} \left\{ \|\widetilde{\mathbf{r}}_{\ell_p,q} - \widetilde{\mathbf{a}}_{\ell_p}^{\text{rot}}\|^2 \right\} \\ \widehat{\mathbf{s}}_{m_p,q} &= \arg \min_{\widetilde{\mathbf{a}}\,\in\,\mathcal{A}^2} \left\{ \|\widetilde{\mathbf{r}}_{m_p,q} - \widetilde{\mathbf{a}}_{m_p}^{\text{rot}}\|^2 \right\} \end{aligned} \tag{23}$$

where $\widetilde{\mathbf{a}}$ is a 2×1 vector of M-QAM constellations drawn from the set $\mathcal{A}^2$, and $\widetilde{\mathbf{a}}_{\ell_p}^{\text{rot}}$ and $\widetilde{\mathbf{a}}_{m_p}^{\text{rot}}$ are obtained from (22) by substituting $\widetilde{\mathbf{a}}$ for $\mathbf{a}$.

IV. SIMULATION RESULTS AND DISCUSSIONS

In this section, the performance results obtained via Monte-Carlo simulations in MATLAB are presented. The performance of the basic MIMO-OFDM system with no pairwise coding is compared with those of three pairwise coding schemes: SC-PWC, SCH-PWC, and the proposed DPWC. Note that SVD precoding is applied in the basic and the PWC configurations. Without loss of generality, a MIMO-OFDM system with $N_\text{R} = N_\text{T} = 4$ is considered for all simulations. Each OFDM frame has a total of 512 SCs, out of which 254 are data-carrying SCs. Also, the simulated LoS MIMO VLC channel gain matrix, $\mathbf{\Gamma}$, is given by Case II of Table III in the Appendix. The channel has a significant level of ill-conditioning (channel correlation) as indicated by its condition number $\eta = 12.95$ dB (ideal case is $\eta = 0$ dB). Since $\mathbf{\Gamma}$ has

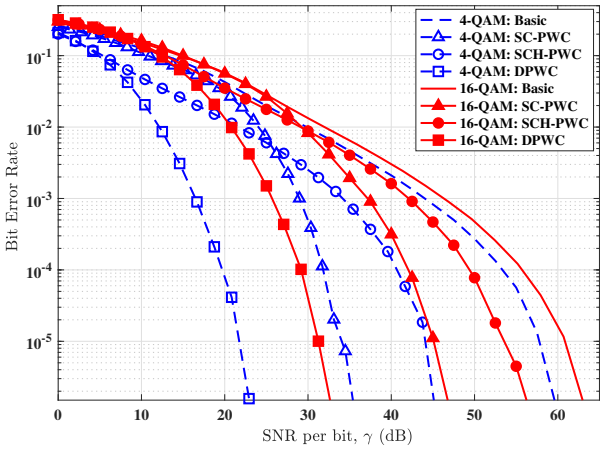

Fig. 5: Error performance of the basic and PWC configurations using 4-QAM and 16-QAM

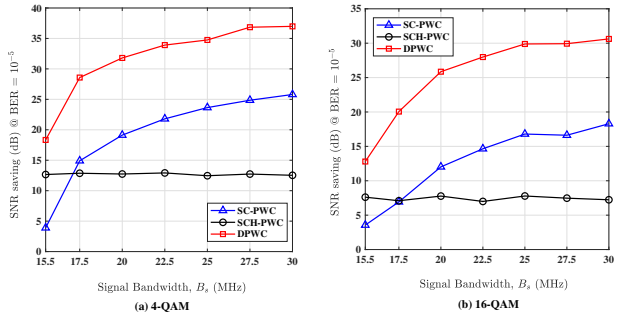

Fig. 6: Performance of PWC schemes for varying signal bandwidth. Plots of SNR savings of PWC schemes over basic MIMO-OFDM versus $B_{\rm s}$ using (a) 4-QAM, (b) 16-QAM.

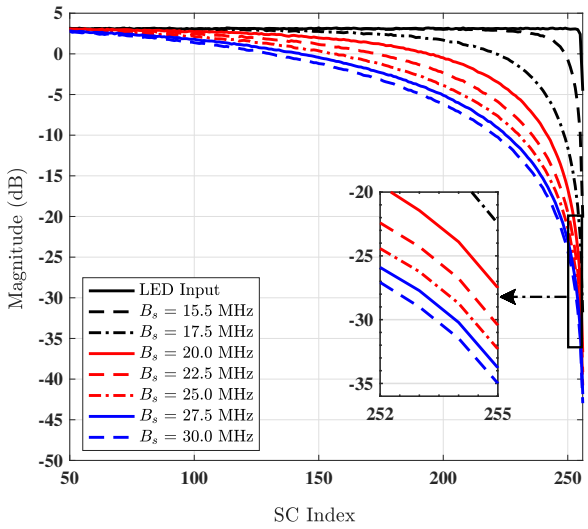

Fig. 7: PSD of LEDs' input signal and LEDs' output signals for different $B_{\rm s}$ values.

a single tap for each MIMO sub-channel, then $\mathbf{H}_k \ \forall\, k$, is equivalent to $\mathbf{\Gamma}$ multiplied by the gain of each SC. However, the value of η is constant for $\mathbf{\Gamma}$ and for $\mathbf{H}_k \ \forall\, k$.

Using 4-QAM and 16-QAM, the plots of the BER versus SNR per bit γ (i.e., energy per bit to noise power spectral density ratio) for the basic and the PWC configurations are depicted in Fig. 5. The signal bandwidth, $B_{\rm s}$ is set at 25 MHz, which is 10 MHz more than the 3-dB bandwidth of the LEDs, (i.e., $B_{\rm LED}$ of 15 MHz). The performance improvement achieved by applying the PWC schemes is apparent from the BER plots. It is observed that the proposed DPWC scheme gives the best performance. For instance, at a representative BER of 10^{-5}, when 4-QAM is used, the DPWC scheme gives an SNR saving of about 37 dB, 23 dB and 12 dB over the basic, SCH-PWC and SC-PWC schemes respectively. A similar result is obtained for 16-QAM where at a BER of 10^{-5}, the DPWC gives about 30 dB, 21 dB an 13 dB in SNR saving over the basic, SCH-PWC and SC-PWC schemes respectively. The SC-PWC scheme is effective in mitigating only the frequency selectivity caused by the LED's limited bandwidth, while the SCH-PWC scheme only addresses the ill-condition (SNR imbalance) due to the VLC MIMO channel correlation. In contrast, the DPWC provides robustness to mitigate the effect of both bandwidth limitation and channel correlation, and hence, the reason for its superior performance.

In Figures 6a and 6b, the performance of the PWC schemes for different $B_{\rm s}$ is shown for 4-QAM and 16-QAM respectively. For each scheme, the SNR savings achieved over the basic system at a BER of 10^{-5} is plotted against $B_{\rm s}$. As expected the DPWC scheme gives the best SNR savings of up to 37 dB and 31 dB at $B_{\rm s}=30$ MHz for 4-QAM and 16-QAM respectively. It can also be observed that the savings achieved by using SCH-PWC scheme is relatively constant for different $B_{\rm s}$ values. This is because in the SCH-PWC scheme, pairing is done among the SCHs only, and thus, SCH-PWC cannot mitigate the SNR imbalance among the SCs due to the LEDs. Hence, the gain achieved over the basic system will only vary significantly if the VLC MIMO channel condition varies. With the $B_{\rm LED}$ = 15 MHz, as $B_{\rm s}$ increases, the number and the attenuation of the SCs beyond the LEDs' 3 dB bandwidth increases. This results in an increased SNR imbalance between the OFDM SCs. The variation in SNR imbalance with $B_{\rm s}$ value is illustrated in Fig. 7 which shows the power spectral density (PSD) of the LEDs' input and output OFDM signal for different $B_{\rm s}$ values. The data-carrying SCs are indexed from 2 to 255. The PSD magnitude is relatively constant for SC index between 2 and 50, hence the reason for their omission in the plots. From Fig. 7, we observe that, as expected, the difference in the SC gain between the least attenuated and the most attenuated SCs increases with the value of $B_{\rm s}$. The highest difference in the gain of the data-carrying SCs range from about 24 dB (for $B_{\rm s}=15.5$ MHz) to about 39 dB (for $B_{\rm s}=30$ MHz).

The performance of the PWC schemes in different VLC channel conditions is depicted in Fig. 8. To portray different levels of signal correlation and therefore different η values, the MIMO VLC channel is simulated using different LED beaming angles Φ. As Φ increases, the emitted light intensity spreads wider which increases the correlation of the LoS channel gain matrix $\mathbf{\Gamma}$, and also reduces the channel gains of each LED-PD link i.e., the diagonal elements of $\mathbf{\Gamma}$. The values of $\mathbf{\Gamma}$ and η obtained for different channel conditions are provided in the Appendix as Table III. The SNR savings achieved at

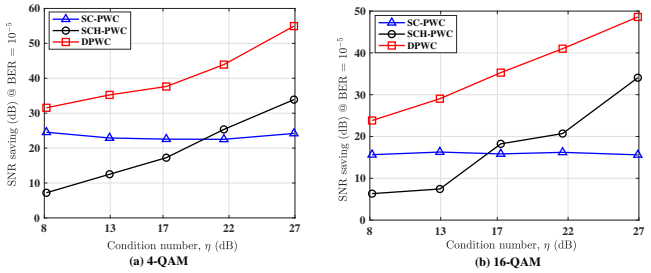

Fig. 8: Performance of the PWC schemes for varying condition number, η. Plots of SNR savings of PWC schemes over basic configuration against η, using (a) 4-QAM, (b) 16-QAM.

a BER of 10^{-5} by the three PWC schemes over the basic configuration are plotted against η in Fig. 8a (using 4-QAM) and Fig. 8b (using 16-QAM). The superior performance of the DPWC scheme is obvious in Fig. 8, since it has the capacity to mitigate SNR imbalance in both the spatial and the spectral domains. For instance, using 4-QAM, DPWC provides an SNR saving of about 21 dB and 31 dB (at $\eta = 26.93$ dB) over the SCH-PWC and SC-PWC schemes respectively. While in the case of 16-QAM, DPWC achieved about 14.5 dB and 33 dB (at $\eta = 26.93$ dB) over the SCH-PWC and SC-PWC schemes respectively. Also, since the SC-PWC scheme only benefits from mitigating SNR imbalance among the SCs, its SNR savings over the basic configuration remains relatively constant for varying η. Though the PWC configurations also suffer from the effect of the increasing channel correlation as η increases, the degradation in performance is less severe compared to the basic configuration. Hence, the reason for the SNR savings achieved by the pairwise coding schemes.

V. EXPERIMENTAL DEMONSTRATION

This section details the experimental setup and results which demonstrates the performance of pairwise coding for MIMO-OFDM VLC system.

A. Experimental Setup

The experimental setup of a 2×2 MIMO-OFDM based VLC system over 1 m link is illustrated by Fig. 9. The LEDs separation is 5 cm while that of the PDs is 7.5 cm. MATLAB® software installed on a personal computer is used to facilitate the digital signal processing (DSP) at the transmitter (TX-DSP) and the receiver (RX-DSP). At the TX, the DSP include generating bit streams, performing bit-to-symbol mapping and S/P conversion of the data symbols. Other TX DSP operations include the DPWC encoding, SVD precoding, IFFT operation, CP insertion and parallel-to-serial (P/S) conversion of the transmit symbols as described in Section III. The data stream are then fed separately to the two channels of the arbitrary waveform generator (AWG) (Agilent 33600A) with sampling rate of 1 GSa/s and up to 120 MHz bandwidth. The waveform generated by the AWG is fed to a Bias-T which diplexes it with a DC bias. The output of the Bias-T is then used to modulate the intensity of the high power blue LEDs (Osram LD CN5M). Focussing lens are deployed at both the transmiting and receiving end of

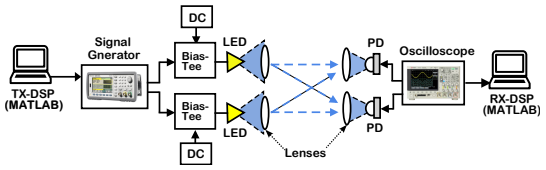

Fig. 9: Experimental setup of 2×2 MIMO-OFDM VLC system.

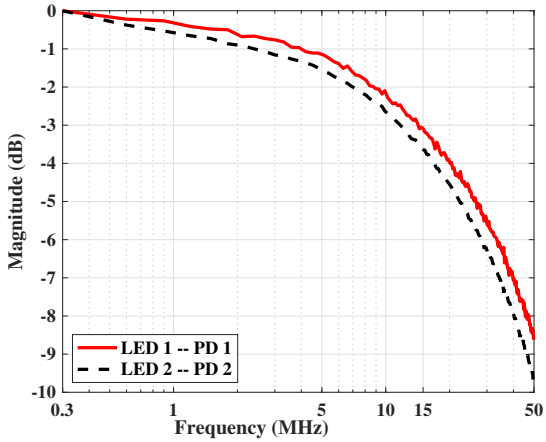

Fig. 10: Frequency responses of the MIMO VLC path between each LED-PD pair

the VLC link to focus the data-bearing optical intensity on the receiving photodiode (PD). Lenses are used to collimate and focus the emitted intensity at the transmitter and the receiver ends respectively.

At the RX, the transmitted signals are detected by the two Si Amplified PDs (Thorlabs PDA10A-EC) which feature built-in low-noise transimpedance amplifier (TIA), Noise equivalent power, NEP $= 3.5 \times 10^{-11}$ W/$\sqrt{\text{Hz}}$. The PDs has an active area of 0.8 mm^2 and a bandwidth of 150 MHz. The output of the PDs are captured on an oscilloscope (Agilent MSO7104B) with sample rate of 4 GSa/s and bandwidth of 1 GHz, and the acquired data is fed back into MATLAB software for offline processing. The DSP at the RX in MATLAB include the FFT operation, LS channel estimation, SVD and pairwise decoding and demodulation of the received symbols.

The data stream sent from each of the two TX channels consists of 10^6 samples, out of which about 50×10^3 are used as synchronisation header and the remaining 950×10^3 as data samples. Each OFDM frame is made up of 512 subcarriers (SCs)/samples - 254 SCs for data symbols, 254 SCs for hermittian symmetry and 4 virtual SCs. With an oversampling factor of 4, this corresponds to $\frac{950000 \times 254}{(4*512)} \approx 117822$ QAM symbols per TX channel. Using 4-QAM, we obtain about 235644 bits per channel. Six different sets of the transmitted data stream are captured at the receiver to get a total of 2.83×10^6 bits for each experimental record.

B. Experimental Results

The frequency responses of the VLC links between each LED-PD pair are shown in Fig. 10. The frequency selective fading caused mainly by the bandwidth limitation of each LEDs is obvious in Fig. 10. The 3-dB bandwidth of both links

TABLE II: Measured LoS channel gain for 2×2 MIMO VLC experimental setup using different LED-PD alignment

CASES	Channel Matrix, Γ	Singular Values	Condition Number, η (dB)
Case A	$\begin{bmatrix}1.0000 & 0.1225\\ 0.0967 & 0.9657\end{bmatrix}$	$\begin{bmatrix}1.0914\\ 0.8746\end{bmatrix}$	0.9620
Case B	$\begin{bmatrix}1.0000 & 0.1502\\ 0.1256 & 0.2648\end{bmatrix}$	$\begin{bmatrix}1.0253\\ 0.2398\end{bmatrix}$	6.3105

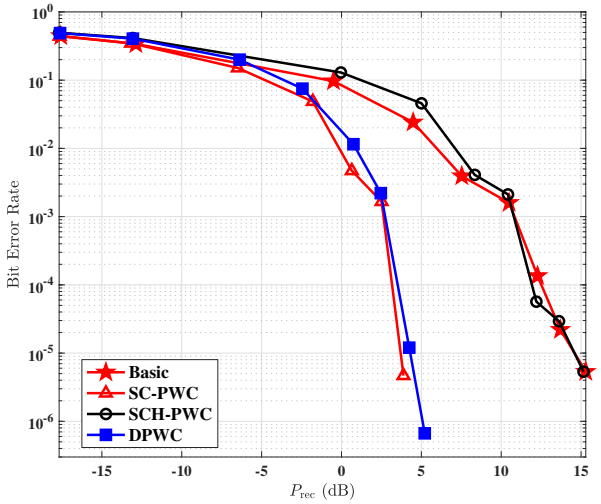

Fig. 11: Experimental BER plots using 4-QAM, Case A: $\eta = 0.9620$ dB, bit rate = 496 Mbps.

is about 12 MHz and 15 MHz respectively. In addition, two different channel conditions, denoted by Cases A and B, are considered using different LED-PD alignment. The estimated and normalised time-domain MIMO VLC channel gain matrices are given in Table II.

Case A represents an almost ideal MIMO configuration in which MIMO channels are less correlated as indicated by the small value of $\eta = 0.9620$ dB. Thus, the major limitation is the bandwidth of the LEDs. At a bit rate of 496 Mbps with 4-QAM, the error performance of the basic and PWC configurations are presented in Fig. 11 with the plot of the BER against the average received electrical power per bit, P_{rec}. It can be seen that both the DPWC and the SC-PWC have superior performance compared to the basic and SCH-PWC. For instance, to achieve a BER of 10^{-4}, the DPWC and the SC-PWC schemes requires about 10 dB less than both the basic and SCH-PWC scheme. We note that due to limited hardware availability, a 2×2 MIMO setup is used for the experiment in contrast to the 4×4 MIMO setup used for the simulation. Also, by comparing Fig. 7 and Fig. 10, we observe that the attenuation incurred by the high-frequency SCs is smaller in the experiment than in the simulation. Hence, the difference in the performance gain achieved in both scenarios. The similarity of the BER plots for the DPWC and the SC-PWC schemes can be attributed to the fact that the MIMO channel is well-conditioned with a small difference in the singular values. Hence, there is no significant gain in applying PWC between the SCHs.

For Case B, the value of $\eta = 6.3105$ dB shows that the MIMO channel experiences some degree of correlation and SNR imbalance in addition to the LEDs' bandwidth limitation. The error performance plots of the basic and PWC configurations at a bit rate of 248 Mbps are presented in Fig. 12. It is observed that the DPWC scheme gives the best performance by employing PWC to reduce the effect of the increased channel correlation. At a BER of 10^{-4}, DPWC provides a power saving of about 5 dB over the SC-PWC and the SCH-PWC, and a power saving of 8 dB over the basic system at BER $= 10^{-3}$. A similar performance trend is seen in Fig. 13 for 496 Mbps where the DPWC again gives the best performance with power saving of about 3.5 dB over the SC-PWC scheme and even significantly higher gain over the SCH-PWC scheme and the basic configuration.

VI. Conclusion

A pairwise coding technique (PWC) termed Dual PWC (DPWC) is proposed for MIMO-OFDM VLC system. The DPWC technique is a technique designed to mitigate the SNR imbalance created in the received information symbols due to the LEDs' bandwidth limitation and the strong correlation of the indoor VLC MIMO channel. This entails the joint coding of information symbol pairs in two degrees of freedom, i.e., spatial and spectral dimensions, of MIMO-OFDM VLC. The overall error performance is improved in terms of error rate, throughput and reliability, without additional power or bandwidth is requirement. The BER plots show that high performance gains are achieved by using DPWC compared the basic MIMO-OFDM. Simulation results show up to 35 dB reduction in SNR requirement (at BER $= 10^{-5}$) when DPWC is applied. Similarly, the experimental results indicate that SNR saving of more 10 dB can be achieved at a data rate of 496 Mbps in a 2×2 MIMO setup using LEDs with 3-dB bandwidth of 12 MHz and 15 MHz. Also, the DPWC scheme is compared with other variants of the PWC techniques in which SNR imbalance is considered in only one of spatial domain (SCH-PWC) or spectral (SC-PWC) domain. Experimental results show that the DPWC achieves up to 5 dB in SNR saving over SC-PWC and more than 10 dB over the SCH-PWC for the same 2×2 MIMO configuration.

Appendix

A. Matrix multiplication form for SC-PWC encoding

Considering two complex QAM constellation symbols $\alpha = \alpha_{\text{r}} + \widehat{i}\alpha_{\text{i}}$ and $\beta = \beta_{\text{r}} + \widehat{i}\beta_{\text{i}}$ to be modulated onto two paired SCs ℓ_1 and m_1 respectively, rotating the symbols by angle ψ yields:

$$\begin{aligned}\alpha_{\text{rot}} &= e^{\widehat{i}\psi}\alpha = (\alpha_{\text{r}}\cos\psi - \alpha_{\text{i}}\sin\psi) + \widehat{i}(\alpha_{\text{r}}\sin\psi + \alpha_{\text{i}}\cos\psi)\\ \beta_{\text{rot}} &= e^{\widehat{i}\psi}\beta = (\beta_{\text{r}}\cos\psi - \beta_{\text{i}}\sin\psi) + \widehat{i}(\beta_{\text{r}}\sin\psi + \beta_{\text{i}}\cos\psi).\end{aligned} \tag{A.24}$$

By exchanging the imaginary part of α_{rot} and the real part of β_{rot}, the interleaved symbols are obtained as:

$$\begin{aligned}\alpha_{\text{int}} &= (\alpha_{\text{r}}\cos\psi - \alpha_{\text{i}}\sin\psi) + \widehat{i}(\beta_{\text{r}}\cos\psi - \beta_{\text{i}}\sin\psi)\\ \beta_{\text{int}} &= (\alpha_{\text{r}}\sin\psi + \alpha_{\text{i}}\cos\psi) + \widehat{i}(\beta_{\text{r}}\sin\psi + \beta_{\text{i}}\cos\psi).\end{aligned} \tag{A.25}$$

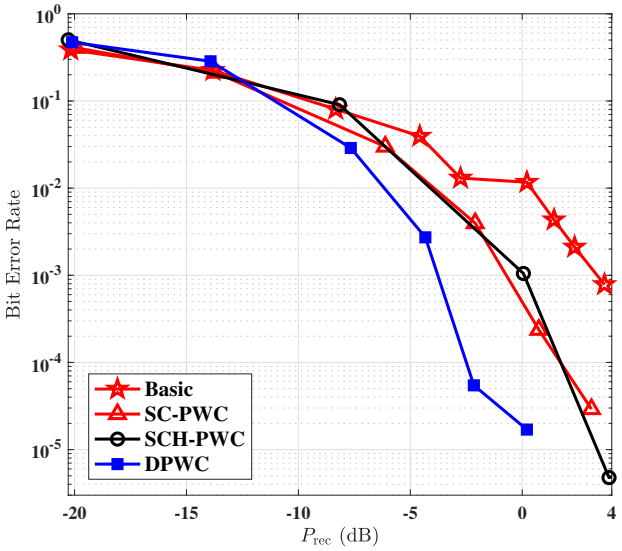

Fig. 12: Experimental BER plots for Case B: $\eta = 6.3105$ dB, bit rate = 248 Mbps, using 4-QAM.

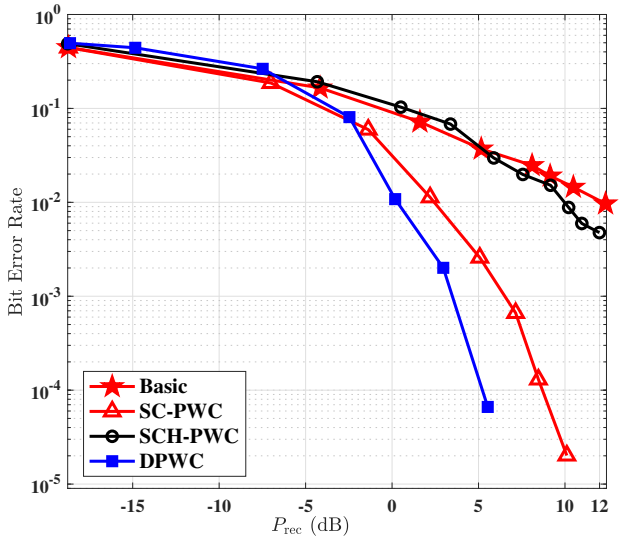

Fig. 13: Experimental BER plots for Case B: $\eta = 6.3105$ dB, bit rate = 496 Mbps, using 4-QAM.

Now, (A.25) can be written in matrix form as:

$$\begin{bmatrix} \Re(\alpha_{\text{int}}) & \Im(\alpha_{\text{int}}) \\ \Re(\beta_{\text{int}}) & \Im(\beta_{\text{int}}) \end{bmatrix} = \begin{bmatrix} \cos\psi & -\sin\psi \\ \sin\psi & \cos\psi \end{bmatrix} \times \begin{bmatrix} \alpha_{\text{r}} & \beta_{\text{r}} \\ \alpha_{\text{i}} & \beta_{\text{i}} \end{bmatrix} \tag{A.26}$$

Thus, the expression in (9) represent a special form of (A.26) for a vector of information symbols.

B. Matrix multiplication form for SCH-PWC encoding

Considering two complex QAM constellation symbols $\alpha = \alpha_{\text{r}} + \widehat{i}\alpha_{\text{i}}$ and $\beta = \beta_{\text{r}} + \widehat{i}\beta_{\text{i}}$ to be modulated onto two paired SCHs c_1 and d_1 respectively, by exchanging the imaginary part of α^{rot} and the real part of β^{rot}, the interleaved symbols are obtained as:

$$\begin{aligned} \alpha_{\text{int}} &= \alpha_{\text{r}} + \widehat{i}\beta_{\text{r}} \\ \beta_{\text{int}} &= \alpha_{\text{i}} + \widehat{i}\beta_{\text{i}}. \end{aligned} \tag{A.27}$$

Rotating the symbols by angle ϕ yields:

$$\begin{aligned} \alpha_{\text{rot}} &= (\alpha_{\text{r}}\cos\phi - \beta_{\text{r}}\sin\phi) + \widehat{i}(\alpha_{\text{r}}\sin\phi + \beta_{\text{r}}\cos\phi) \\ \beta_{\text{rot}} &= (\alpha_{\text{i}}\cos\phi - \beta_{\text{i}}\sin\phi) + \widehat{i}(\alpha_{\text{i}}\sin\phi + \beta_{\text{i}}\cos\phi). \end{aligned} \tag{A.28}$$

Then, by exchanging the imaginary part of α^{rot} and the real part of β^{rot}, the new interleaved symbols are obtained as:

$$\begin{aligned} \widehat{\alpha}_{\text{int}} &= (\alpha_{\text{r}}\cos\phi - \beta_{\text{r}}\sin\phi) + \widehat{i}(\alpha_{\text{i}}\cos\phi - \beta_{\text{i}}\sin\phi) \\ &= (\alpha_{\text{r}} + \widehat{i}\alpha_{\text{i}})\cos\phi - (\beta_{\text{r}} + \widehat{i}\beta_{\text{i}})\sin\phi \\ \widehat{\beta}_{\text{int}} &= (\alpha_{\text{r}}\sin\phi + \beta_{\text{r}}\cos\phi) + \widehat{i}(\alpha_{\text{i}}\sin\phi + \beta_{\text{i}}\cos\phi) \\ &= (\alpha_{\text{r}} + \widehat{i}\alpha_{\text{i}})\cos\phi + (\beta_{\text{r}} + \widehat{i}\beta_{\text{i}})\sin\phi \end{aligned} \tag{A.29}$$

Now, (A.29) can be written in matrix form as:

$$\begin{bmatrix} \widehat{\alpha}_{\text{int}} \\ \widehat{\beta}_{\text{int}} \end{bmatrix} = \begin{bmatrix} \cos\phi & -\sin\phi \\ \sin\phi & \cos\phi \end{bmatrix} \times \begin{bmatrix} \alpha \\ \beta \end{bmatrix} \tag{A.30}$$

Thus, the expression in (11) is equivalent to (A.26).

C. MIMO VLC LoS channel impulse response

TABLE III: VLC LoS channel gain for 4×4 MIMO setup using different LED beaming angles

CASES	LED Beaming Angle, Φ	Channel Matrix, Γ $\times 10^{-4}$	Singular Values $\times 10^{-4}$	Condition Number η (dB)
Case I	15°	$\begin{bmatrix} 1.1650 & 0.5880 & 0.5880 & 0.2950 \\ 0.5170 & 1.4140 & 0.1860 & 0.5170 \\ 0.6410 & 0.2410 & 1.2890 & 0.4640 \\ 0.2410 & 0.4640 & 0.6410 & 1.2890 \end{bmatrix}$	$\begin{bmatrix} 2.6357 \\ 1.1535 \\ 0.9778 \\ 0.4030 \end{bmatrix}$	8.16
Case II	20°	$\begin{bmatrix} 0.7776 & 0.5616 & 0.5616 & 0.4002 \\ 0.4938 & 0.9436 & 0.2532 & 0.4938 \\ 0.6125 & 0.3267 & 0.8606 & 0.4429 \\ 0.3267 & 0.4429 & 0.6125 & 0.8606 \end{bmatrix}$	$\begin{bmatrix} 2.2434 \\ 0.6311 \\ 0.4806 \\ 0.1139 \end{bmatrix}$	12.95
Case III	25°	$\begin{bmatrix} 0.5419 & 0.4620 & 0.4620 & 0.3874 \\ 0.4062 & 0.6575 & 0.2451 & 0.4062 \\ 0.5039 & 0.3163 & 0.5997 & 0.3644 \\ 0.3163 & 0.3644 & 0.5039 & 0.5997 \end{bmatrix}$	$\begin{bmatrix} 1.7850 \\ 0.3685 \\ 0.2500 \\ 0.0365 \end{bmatrix}$	17.25
Case IV	30°	$\begin{bmatrix} 0.3966 & 0.3700 & 0.3700 & 0.3389 \\ 0.3253 & 0.4812 & 0.2144 & 0.3253 \\ 0.4035 & 0.2767 & 0.4389 & 0.2918 \\ 0.2767 & 0.2918 & 0.4035 & 0.4389 \end{bmatrix}$	$\begin{bmatrix} 1.4117 \\ 0.2350 \\ 0.1457 \\ 0.0097 \end{bmatrix}$	21.61
Case V	35°	$\begin{bmatrix} 0.3026 & 0.2981 & 0.2981 & 0.2880 \\ 0.2621 & 0.3672 & 0.1822 & 0.2621 \\ 0.3251 & 0.2351 & 0.3349 & 0.2351 \\ 0.2351 & 0.2351 & 0.3251 & 0.3349 \end{bmatrix}$	$\begin{bmatrix} 1.1310 \\ 0.1619 \\ 0.0958 \\ 0.0023 \end{bmatrix}$	26.93

REFERENCES

[1] Z. Ghassemlooy, W. Popoola, and S. Rajbhandari, *Optical wireless communications: system and channel modelling with Matlab®*. CRC Press, 2012.

[2] D. Karunatilaka, F. Zafar, V. Kalavally, and R. Parthiban, "LED Based Indoor Visible Light Communications: State of the Art," *IEEE Communications Surveys & Tutorials*, vol. 17, no. 3, pp. 1649–1676, 2015.

[3] H. G. Olanrewaju, F. B. Ogunkoya, and W. O. Popoola, "Spatial Modulation - A Low Complexity Modulation Technique for Visible Light Communications," in *Visible Light Communications*, J.-Y. Wang, Ed. Rijeka: IntechOpen, 2017, ch. 1. [Online]. Available: https://doi.org/10.5772/intechopen.68888

[4] H. Burchardt, N. Serafimovski, D. Tsonev, S. Videv, and H. Haas, "VLC: Beyond point-to-point communication," *IEEE Communications Magazine*, vol. 52, no. 7, pp. 98–105, 2014.

[5] A. Nuwanpriya, S.-W. Ho, and C. S. Chen, "Indoor MIMO visible light communications: Novel angle diversity receivers for mobile users," *IEEE Journal on Selected Areas in Communications*, vol. 33, no. 9, pp. 1780–1792, 2015.

[6] S. H. Lee, K.-I. Ahn, and J. K. Kwon, "Multilevel transmission in dimmable visible light communication systems," *Journal of Lightwave Technology*, vol. 31, no. 20, pp. 3267–3276, 2013.

[7] W. O. Popoola, Z. Ghassemlooy, and B. G. Stewart, "Pilot-assisted PAPR reduction technique for optical OFDM communication systems," *Journal of Lightwave Technology*, vol. 32, no. 7, pp. 1374–1382, 2014.

[8] T. Fath and H. Haas, "Performance comparison of MIMO techniques for optical wireless communications in indoor environments," *IEEE Transactions on Communications*, vol. 61, no. 2, pp. 733–742, 2013.

[9] H. G. Olanrewaju, J. Thompson, and W. O. Popoola, "Performance of optical spatial modulation in indoor multipath channel," *IEEE Transactions on Wireless Communications*, 2018.

[10] K.-H. Park, Y.-C. Ko, and M.-S. Alouini, "On the power and offset allocation for rate adaptation of spatial multiplexing in optical wireless MIMO channels," *IEEE Transactions on Communications*, vol. 61, no. 4, pp. 1535–1543, 2013.

[11] Y. Hong, T. Wu, L.-K. Chen *et al.*, "On the performance of adaptive MIMO-OFDM indoor visible light communications," *IEEE Photonics Technology Letters*, vol. 28, no. 8, pp. 907–910, 2016.

[12] D. Tse and P. Viswanath, *Fundamentals of Wireless Communication*. Cambridge university press, 2005.

[13] S. K. Mohammed, E. Viterbo, Y. Hong, and A. Chockalingam, "MIMO Precoding With X-and Y-codes," *IEEE Transactions on Information Theory*, vol. 57, no. 6, pp. 3542–3566, 2011.

[14] J. Boutros and E. Viterbo, "Signal Space Diversity: A Power-and Bandwidth-efficient Diversity Technique for the Rayleigh Fading Channel," *IEEE Transactions on Information theory*, vol. 44, no. 4, pp. 1453–1467, 1998.

[15] Y. Hong, A. J. Lowery, and E. Viterbo, "Sensitivity Improvement and Carrier Power Reduction in Direct-Detection Optical OFDM Systems by Subcarrier Pairing," *Optics express*, vol. 20, no. 2, pp. 1635–1648, 2012.

[16] C. Zhu, B. Song, L. Zhuang, B. Corcoran, and A. J. Lowery, "Subband Pairwise Coding for Robust Nyquist-WDM Superchannel Transmission," *Journal of Lightwave Technology*, vol. 34, no. 8, pp. 1746–1753, 2016.

[17] B. Song, B. Corcoran, Q. Wang, L. Zhuang, and A. J. Lowery, "Subcarrier pairwise coding for short-haul L/E-ACO-OFDM," *IEEE photonics technology letters*, vol. 29, no. 18, pp. 1584–1587, 2017.

[18] I. N. Osahon, C. Ziyan, T. Adiono, and W. O. Popoola, "SI-POF transmission with OFDM and sub-carrier pairwise coding," in *2018 7th IEEE International Conference on Performance Evaluation and Modeling in Wired and Wireless Networks (PEMWN)*, Sept 2018.

[19] S. Althunibat and R. Mesleh, "Enhancing spatial modulation system performance through signal space diversity," *IEEE Communications Letters*, vol. 22, no. 6, pp. 1136–1139, 2018.

[20] S. Özyurt and O. Kucur, "Zero-forcing beamforming with signal space diversity," *IEEE Transactions on Vehicular Technology*, vol. 67, no. 1, pp. 812–816, 2018.

[21] G. Krishna, K. V. Srinivas, S. Bhashyam, and R. D. Koilpillai, "Signal space diversity for spatial multiplexing," in *2008 IEEE 19th International Symposium on Personal, Indoor and Mobile Radio Communications*. IEEE, 2008, pp. 1–5.

[22] Z. Wu and X. Gao, "Improved MIMO-OFDM scheme for the next generation WLAN," *Journal of Systems Engineering and Electronics*, vol. 24, no. 1, pp. 52–59, 2013.

[23] C. Zhu, B. Song, B. Corcoran, L. Zhuang, and A. J. Lowery, "Improved Polarization Dependent Loss Tolerance for Polarization Multiplexed Coherent Optical Systems by Polarization Pairwise Coding," *Optics Express*, vol. 23, no. 21, pp. 27 434–27 447, 2015.

[24] J. He and J. Shi, "An enhanced adaptive scheme with Pairwise Coding for OFDM-VLC system," *IEEE Photonics Technology Letters*, 2018.

[25] P. S. Diniz, *Adaptive filtering*. Springer, 1997.

[26] J. Armstrong, "OFDM for optical communications," *Journal of lightwave technology*, vol. 27, no. 3, pp. 189–204, 2009.

[27] H. Le Minh, D. O'Brien, G. Faulkner, L. Zeng, K. Lee, D. Jung, Y. Oh, and E. T. Won, "100-Mbps NRZ visible light communications using a postequalized white LED," *IEEE Photonics Technology Letters*, vol. 21, no. 15, pp. 1063–1065, 2009.

[28] G. Egecan, K. O. Akande, P. Anthony Haighy, and W. O. Popoola, "Frequency response modelling of cool and warm white leds in vlc systems," in *First Regional Wireless Communication Center of Western Asia*. Isfahan University of Technology, 2017.

[29] J. R. Barry, J. M. Kahn, W. J. Krause, E. A. Lee, D. G. Messerschmitt *et al.*, "Simulation of multipath impulse response for indoor wireless optical channels," *IEEE journal on selected areas in communications*, vol. 11, no. 3, pp. 367–379, 1993.